

Circumstellar dust shells around long-period variables

VII. The role of molecular opacities

Ch. Helling¹, J.M. Winters^{1,2}, and E. Sedlmayr¹

¹ Institut für Astronomie und Astrophysik, TU Berlin, Sekr. PN 8-1, Hardenbergstrasse 36, 10623 Berlin, Germany

² Max-Planck-Institut für Radioastronomie, Auf dem Hügel 69, 53121 Bonn, Germany

Received 10 October 1999 / Accepted 7 March 2000

Abstract. The role of molecular opacities for the structure and dynamics of winds of carbon-rich AGB stars is investigated in the frame work of time-dependent hydrodynamic models of dust forming circumstellar shells around cool pulsating stars. New Rosseland and Planck mean gas opacity tables have been calculated for $T \in [500\text{K}, 10\,000\text{K}]$ and $n_{\text{(H)}} \in [10^5\text{cm}^{-3}, 10^{15}\text{cm}^{-3}]$ for solar, LMC and SMC abundances. Carbon-rich, static and time-dependent models have been computed using either the Planck mean or the Rosseland mean for solar and LMC metallicity or a constant gas opacity ($\chi^{\text{g}} = 2 \cdot 10^{-4}\text{cm}^2\text{g}^{-1}$, Bowen 1988). In the model calculations, a large gas opacity (Planck mean) generally causes a less dense atmosphere than a small gas opacity (Rosseland mean, constant gas opacity) which leads to smaller amounts of dust formed, and consequently to smaller mass loss rates $\langle \dot{M} \rangle$, lower terminal wind velocities $\langle v_{\infty} \rangle$ and lower dust-to-gas ratios $\langle \rho_{\text{dust}} / \rho_{\text{gas}} \rangle$. Models with lower metallicity (LMC) form by far the smallest amount of dust and show therefore the lowest $\langle \dot{M} \rangle$, $\langle v_{\infty} \rangle$, and $\langle \rho_{\text{dust}} / \rho_{\text{gas}} \rangle$. Counteracting to the global density reduction due to strong gas absorption, the density might *LOCALLY* increase due to a pressure inversion. These pressure inversions are preserved even in the hydrodynamic models where the atmosphere is disturbed by the propagation of shock waves. Due to the present determination of the temperature structure by grey opacities in the time-dependent models, the occurrence of pressure inversions deserves, however, further investigations by means of a more elaborate treatment of the radiative transfer in dynamic model atmospheres.

Key words: infrared: stars – molecular processes – hydrodynamics – stars: late-type – stars: circumstellar matter

1. Introduction

Strong gas opacities due to ionic and atomic lines play a decisive role as a possible wind initiator in hot stellar winds (e.g. Cas-tor et al. 1975; Pauldrach et al. 1986). In cool stars, molecules possess a large potential of absorbing radiation due to their rich line spectra and might thereby influence the hydrodynamics by a

possibly large radiation pressure. Investigations have been performed regarding this effect in the framework of hydrostatic models (e.g. Jørgensen & Johnson 1992), some in stationary models of supergiants (e.g. Achmad et al. 1997) and Miras (e.g. Maciel 1976) and in time-dependent model atmospheres of AGB stars (Höfner et al. 1998).

Asplund (1998) has shown in hydrostatic models of hydrogen-deficient stars that the gas opacity can locally be large enough to cause the radiative acceleration to exceed the gravitational deceleration ($a_{\text{rad}}/g = \alpha > 1$) which results in a pressure inversion in the very inner parts of these models. Achmad et al. (1997) discuss the presence of pressure inversions in stationary models of supergiants using as initial values the static model atmospheres of Kurucz (1979 in an updated version). Jørgensen & Johnson (1992) however, argued by means of hydrostatic calculations that the opacity data available can not produce $\alpha > 1$. Höfner et al. (1998) concluded that molecular gas opacities can contribute to the generation of the wind in time-dependent model atmospheres where the gas opacity has been approximated by Planck mean values.

The radiative acceleration $a_{\text{rad}} = (4\pi/c)\chi_{\text{H}}H$ is especially important if a_{rad} exceeds the local gravitational deceleration g , because it becomes the dominant force in the equation of motion in this case. The determination of the flux weighted mean extinction coefficient χ_{H} (and the intensity weighted mean χ_{J}) requires the knowledge of the exact frequency distribution of the radiation field at each point in the atmosphere. In the grey approximation of the radiative transfer equation $\chi_{\text{H}} = \chi_{\text{J}} = \chi$. In hot and dense regions of the atmosphere, where the mean free path of all photons of arbitrary wavelength is smaller than the characteristic scale height of the medium, the diffusion approximation holds for the radiative flux which implies $\chi_{\text{H}} = \chi_{\text{Ross}}$, where χ_{Ross} is the Rosseland mean extinction coefficient. In the outer parts of the atmosphere and in the circumstellar envelope, the gas becomes optically thin and the diffusion approximation is no longer valid. Moreover, single, strongly absorbing frequencies become important and determine thereby the flux mean extinction coefficient χ_{H} as well as the intensity weighted mean χ_{J} and the Planck mean χ_{Planck} which both enter into the evaluation of the local temperature. In the limiting case of a missing correlation between the frequency distribution of the flux and the frequency distribution of the opacity, χ_{H} may ap-

proximately be replaced by χ_{Planck} in order to determine the radiative acceleration and may be used as a tool to study the UPPER LIMIT of the effects molecules can have on the structure of extended atmospheres. In case of dust formation in the atmosphere, the matter becomes optical thick and the radiation field tends to be locally Planckian. In contrast, models computed with Rosseland means χ_{Ross} can serve as the LOWER LIMIT regarding the evaluation of the radiative acceleration.

The influence of the frequency dependence of the molecular opacities has been demonstrated by several workers (e.g. Sneden & Johnsen et al. 1976; Helling & Jørgensen 1998) and large deviations in the temperature structure of hydrostatic models have been noticed. Such investigations do, however, very likely underestimate the radiative acceleration in the time-dependent hydrodynamic case since velocity fields are present and lines may be Doppler-shifted to neighbouring frequencies where flux can escape from the inner layers. For example, a hydrodynamic velocity of $u = 20 \text{ km s}^{-1}$ causes a line to be shifted up to about 8 Doppler widths from its original position in a turbulent medium with $v_{\text{turb}} = 2.5 \text{ km s}^{-1}$. However, it is still not possible to compute a consistent hydrodynamic stellar atmosphere model including Doppler shifted line absorption with today's computer capacities. First investigations with respect to a frequency dependent treatment of the molecular opacity in dynamic model atmospheres have been presented by Höfner (1999) where dust formation has been left out because of the computational effort.

In most of the time-dependent hydrodynamic models presented so far a constant gas opacity $\chi^{\text{g}} = 2 \cdot 10^{-4} \text{ cm}^2 \text{ g}^{-1}$ has been used (e.g. Bowen 1988; Fleischer et al. 1992; Feuchtinger et al. 1993; Winters et al. 1997; Höfner & Dorfi 1997). This value is based on Rosseland mean gas opacities published by Alexander et al. (1983) and has been chosen by Bowen (1988) as a representative value for the gas opacity in the stellar photosphere. Time-dependent models computed with this constant gas opacity may also serve as a lower limit since the value $2 \cdot 10^{-4} \text{ cm}^2 \text{ g}^{-1}$ is rather small. These models are similar to the models computed with variable Rosseland means regarding the resulting hydrodynamic structure.

In Sect. 2, we discuss the opacity calculation and show the differences arising from various metallicities. Sect. 3 contains a short description of the hydrodynamic model code used. In Sect. 4, results regarding the influence of the molecular opacities on the hydrodynamic and the dust structure of the circumstellar shell (CS) and regarding the wind properties are presented. In Sect. 5, the occurrence of pressure inversions is investigated. We demonstrate that pressure inversions occur even under pulsational disturbances in our time-dependent models. In Sect. 6, the wind properties are discussed regarding piston amplitude and C/O ratio. A discussion of the pressure inversions contain this section. Sect. 7 summarises the conclusions of this paper.

2. Molecular mean opacities

2.1. Chemical and opacity data

Our opacity treatment is based on the MARCS model atmosphere code (Gustafsson et al. 1975; Jørgensen et al. 1992) in

the version of Helling & Jørgensen (1998) and has been combined with a new equilibrium chemistry. The chemical equilibrium constants, K_p , are mainly those used in Gail & Sedlmayr (1986) but for TiO, TiO₂, Ti⁺, C₃, Si⁺, S⁺, Fe⁺, new polynomial fits to the thermo-chemical data given in the JANAF tables (Chase et al. 1985) have been performed. Coefficients for C₃H and TiS were taken from Tsuji (1973), and those for TiC were kindly provided by Gauger (1997, priv. comm., see Appendix B). The equilibrium constants K_p given in Tsuji (1973) and those obtained from the JANAF tables can strongly differ at low temperatures due to new thermodynamic data regarding molecular dissociation constants. For instance, the different equilibrium constants for TiO₂ result in differences of the TiO number density of up to three orders of magnitude. Differences of about two orders of magnitude in the number density has been found for C₃ and about one order of magnitude in the number density of HCN and of C₂.

Our Planck mean and Rosseland mean gas opacities are based on Opacity Sampling data of several millions of spectral lines of CO (Goorvitch 1994), TiO (Jørgensen 1994a), SiO (Langhoff & Bauschilder 1993), H₂O (Jørgensen & Jensen 1993), CH (Jørgensen et al. 1996), CN (Jørgensen & Larsson 1990) C₂ (Jørgensen 1996), C₃ (Jørgensen et al. 1989), HCN and C₂H₂ (Jørgensen 1990 in an updated version) beside continuum absorption from HI (Karzas & Latter 1961), H⁻ (John 1988), H+H (Doyle 1968), H₂⁻ (Somerville 1964), H₂⁺ (Mihalas 1965), HeI (Peach 1970), He⁻ (Carbon et al. 1969), and CI, MgI, AlI, and SiI (Peach 1970). Thomson scattering and Rayleigh scattering for HI and HeI (Dalgarno 1962) are included. Scattering has been included both, in $\chi_{\text{Ross}}^{\text{g}}$ and in $\chi_{\text{Planck}}^{\text{g}}$.

2.2. Mean gas opacities in the ($T, n_{\text{(H)}}$) plane

Rosseland and Planck mean gas opacities have been computed for the element abundances of the Sun (C/O=0.43) and for an enhanced carbon abundance (C/O=1.8) in the temperature range $T \in [500 \text{ K}, 10\,000 \text{ K}]$ and for total hydrogen densities $n_{\text{(H)}} \in [10^5 \text{ cm}^{-3}, 10^{15} \text{ cm}^{-3}]$. In addition, tables for the element abundances of the Large and the Small Magellanic Cloud have been calculated (see Table A.1). All opacity species (CO, TiO, SiO, H₂O, CH, CN, C₂, C₃, HCN, C₂H₂, and continuum opacities) have been included in the calculation irrespective of the C/O ratio.

The overall structure of Planck mean and Rosseland mean gas opacities in the ($T, n_{\text{(H)}}$) plane is characterised by the interplay between continuum opacities and molecular line opacities (Fig. 1). The mean gas opacities decrease towards low temperatures unless the temperature is so low that molecules are present. At high temperatures ($T > 6000 \text{ K}$), the main contributions for both kinds of mean gas opacities are from the continuum species. At low densities, scattering is the main continuum source. In an intermediate temperature range ($3000 \text{ K} \lesssim T \lesssim 1500 \text{ K}$, depending on the density), the increasing number densities of molecular opacity species cause an increase in both mean gas opacities. At $T < 1500 \text{ K}$, the number densities of most of the

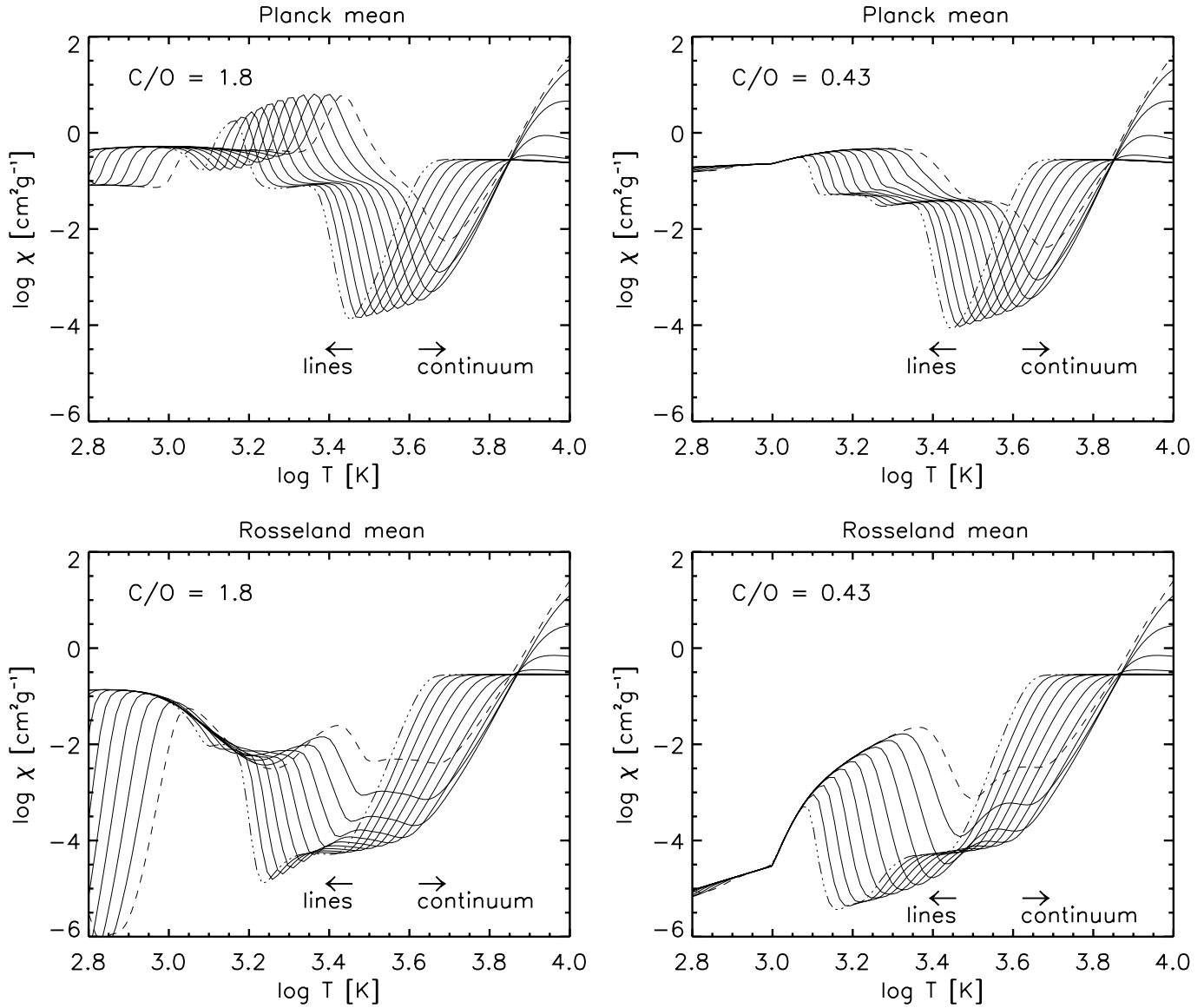


Fig. 1. Planck mean (upper panels) and Rosseland mean (lower panels) gas opacities for a solar gas composition ($C/O=0.43$, r.h.s.) and a gas of an enhanced carbon abundance ($C/O=1.8$, l.h.s.). The dashed lines indicate opacities at the smallest ($\rho = 2.3 \cdot 10^{-19} \text{ g cm}^{-3}$) and the dash-dotted line at the largest ($\rho = 2.3 \cdot 10^{-9} \text{ g cm}^{-3}$) density tabulated.

considered line opacity molecules decrease again. Instead, more complex molecules like CH_4 , NH_3 or CO_2 are present which are not considered here as a source of opacity due to the lack of data. The contributions at the lowest temperatures are mainly provided by H_2^- (f-f) continuum absorption and by CO (but also SiO, H_2O) for a carbon-rich chemistry and by H_2^- (f-f), SiO and H_2O in an oxygen-rich chemistry.

The Planck mean gas opacities are always larger than the Rosseland means by at least one order of magnitude at the same temperature T and total density ρ if the line opacity is dominant. This difference increases towards lower temperatures. The reason for this behaviour lies within the nature of the averaging processes: while the Planck mean is dominated by strong absorption lines of the molecules, the Rosseland mean is dominated by the transparent spectral regions.

The influence of the oxygen bearing opacity species (TiO, SiO and H_2O) in the carbon-rich case and of the carbon bearing opacity species (CH, CN, C_2 , C_3 , HCN, C_2H_2) in the oxygen-rich case on the mean gas opacities has been investigated. The oxygen containing opacity species affect the carbon-rich mean opacity at low temperatures ($T < 1000 \text{ K}$) were the TiO, SiO and H_2O concentrations increase but those of diatomic carbon molecules decrease, a difference of about 0.5 dex occurs for the Planck mean gas opacities. The effect is independent of the gas density and negligible for Rosseland mean gas opacities which are dominated by the continuum and the weak line opacity. In contrast, the neglect of CH, CN, C_2 , C_3 , HCN, and C_2H_2 in the oxygen-rich case does not influence the mean gas opacities in the parameter range investigated here.

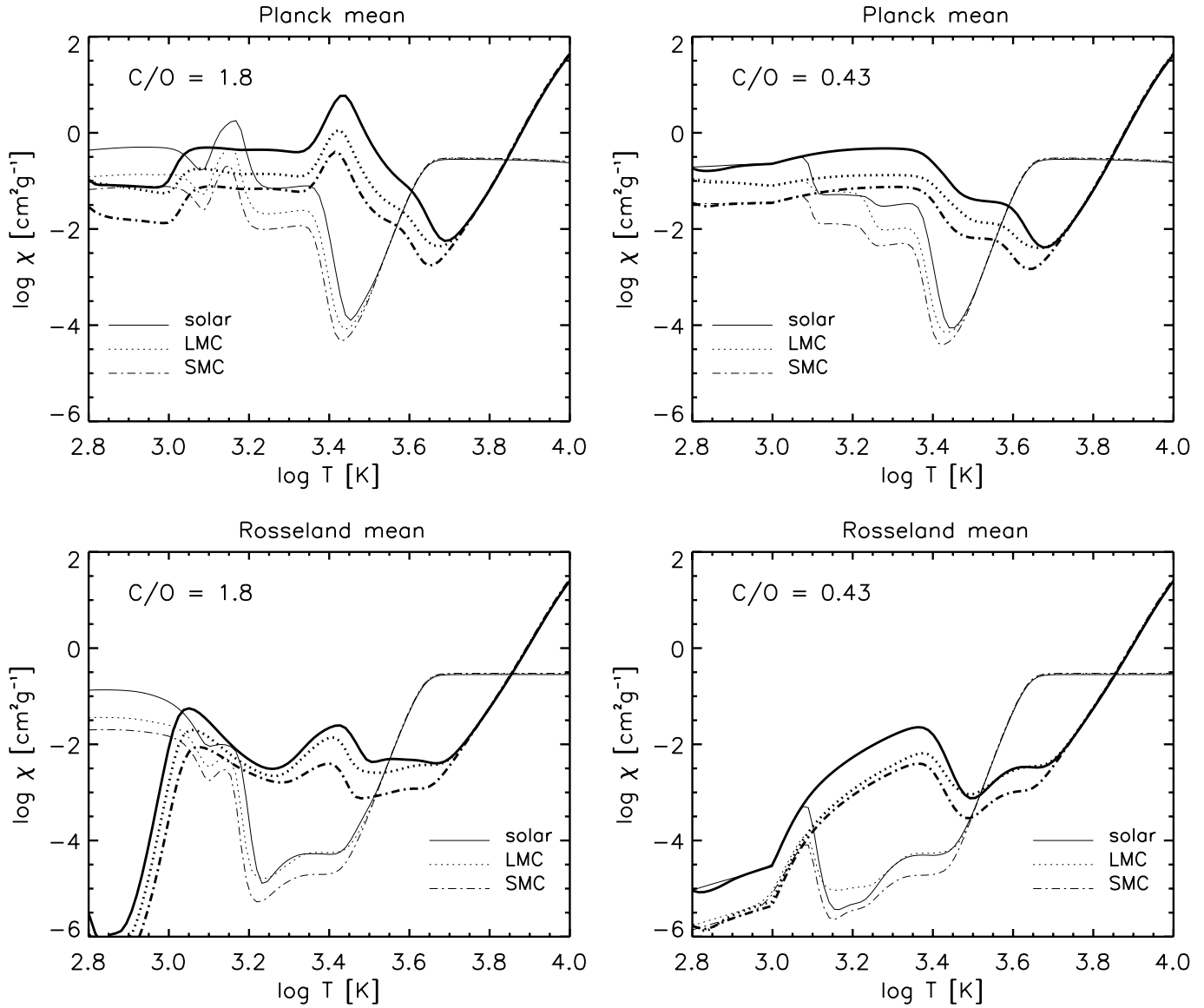


Fig. 2. Planck mean (upper panels) and Rosseland mean (lower panels) gas opacities for a carbon-rich ($C/O=1.8$, l.h.s.) and an oxygen-rich ($C/O=0.43$, r.h.s.) gas for different metallicities. Solid line – solar, dotted line – LMC, dashed line – SMC gas composition. Thin lines indicate opacities at the smallest ($\rho = 2.3 \cdot 10^{-19} \text{ g cm}^{-3}$) and thick lines at the largest ($\rho = 2.3 \cdot 10^{-9} \text{ g cm}^{-3}$) density tabulated.

2.3. Mean gas opacities for different metallicities

Rosseland mean and Planck mean gas opacities have also been computed for the element abundances of the Large and the Small Magellanic Cloud (LMC and SMC) for a carbon-rich ($C/O=1.8$) and an oxygen-rich ($C/O=0.43$) gas composition in the same temperature and total hydrogen density range ($T \in [500\text{K}, 10\,000\text{K}]$, $n_{\text{H}} \in [10^5 \text{cm}^{-3}, 10^{15} \text{cm}^{-3}]$).

The comparison of mean gas opacities for solar, LMC and SMC element abundances (see Table A.1) is depicted in Fig. 2 for a small ($\rho = 2.3 \cdot 10^{-19} \text{ g cm}^{-3}$) and a large ($\rho = 2.3 \cdot 10^{-9} \text{ g cm}^{-3}$) density. The mean opacities of a gas of solar composition are – independent of the carbon overabundance – almost always larger than the mean gas opacities resulting for the smaller element abundances of the LMC and the

SMC for the opacity species considered here. The reason is the increasing number density of the opacity species with increasing metallicity. In comparison to the opacities calculated for solar element abundances, the mean gas opacities for the SMC show the largest differences, since the element abundances deviate the most. The large similarity at high temperatures is caused by the very similar element abundances of the main continuum absorption species H and He. The mean LMC gas opacities are more similar to the solar mean gas opacities at lower temperature than the mean SMC gas opacities. The reason is the similarity between the solar and the LMC element abundances of the continuum species Mg (Al and K were assumed to be solar for the LMC) beside H and He. Also the LMC element abundances of Si, O, and C are more similar to the solar values than the SMC abundances.

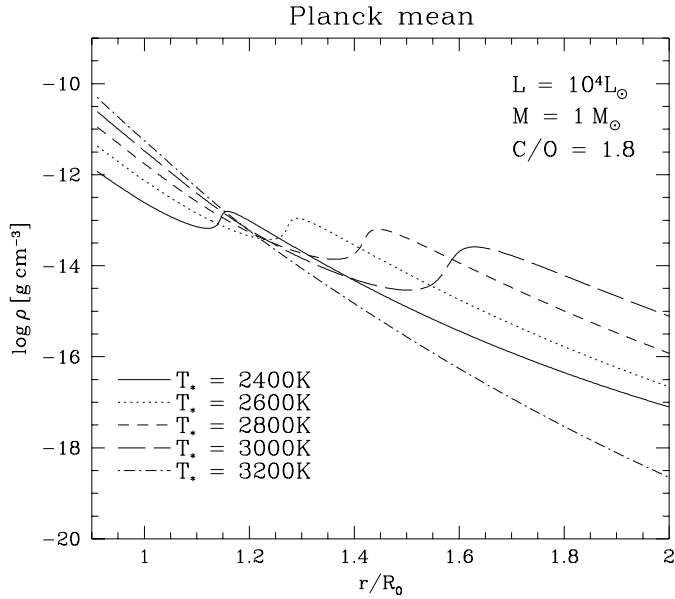


Fig. 3. Density versus radial distance in units of the initial stellar radius R_0 of a sequence of hydrostatic models computed with Planck mean gas opacities

3. Model calculations

Time-dependent models of carbon-rich dynamic atmospheres of AGB stars with solar and with LMC element abundances have been calculated by means of the CHILD-code developed by Fleischer et al. (1992). The code solves the coupled equation system describing time-dependent hydrodynamics, radiative transfer, chemistry, and dust formation. Dust nucleation, growth and evaporation are treated by means of the moment method developed by Gail et al. (1984), Gail & Sedlmayr (1988) and Gauger et al. (1990). The molecular composition of the gas is calculated assuming chemical equilibrium and the interior pulsation of the star is simulated by a sinusoidal variation of the innermost grid point R_{inner} with period P and amplitude Δu . The radiative transfer problem is solved in grey approximation applying the Unno-Kondo method (Unno & Kondo 1976; 1977; Hashimoto 1995; see Winters et al. 1997 for details). In contrast to Fleischer et al. (1992), the flux weighted mean gas opacities, $\chi_{\text{H}}^{\text{g}}$, have been approximated by the above discussed new Rosseland or Planck mean gas opacities, respectively. For comparison, also models with a constant gas opacity ($\chi_{\text{const}}^{\text{g}} = 2 \cdot 10^{-4} \text{cm}^2 \text{g}^{-1}$, Bowen 1988) have been computed. The mean dust opacities are the same for all models, namely the fit to the Rosseland mean dust opacity given in Gail & Sedlmayr (1985) ($Q_{\text{Ross,C}}^{\text{d}}(T) = 5.9 T$).

The mean molecular weight $\mu = \sum m_i n_i / \sum n_i$ is kept constant in the hydrodynamic model calculations.

The initial values for the solution of the system of partial differential equations describing the full atmosphere problem is taken to be hydrostatic and dust-free, and it is determined by the stellar temperature T_* , the stellar luminosity L_* , the stellar mass M_* , the carbon-to-oxygen ratio C/O and the remaining element abundances ϵ_i . For the time-dependent calculations, the

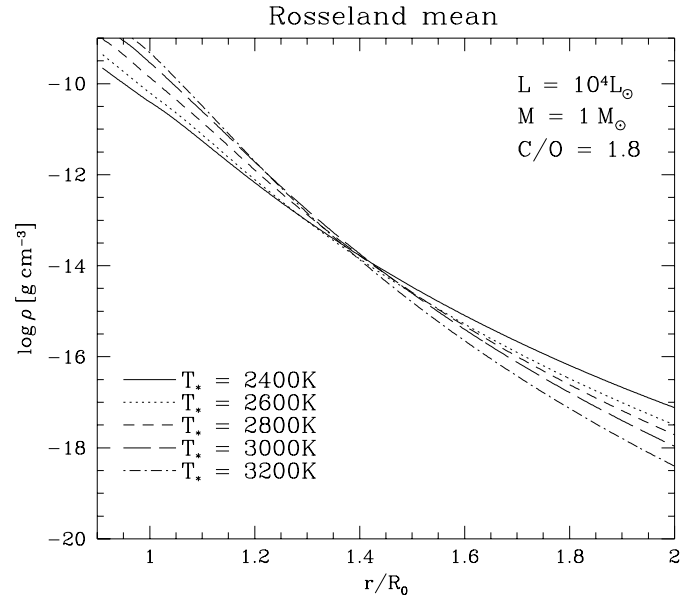


Fig. 4. Density versus radial distance in units of the initial stellar radius R_0 of a sequence of hydrostatic models computed with Rosseland mean gas opacities

piston period P and the piston amplitude Δu are additionally prescribed.

4. Results

4.1. Initial models

The initial models, i.e. the dust-free, static solution of the equation of motion and the equation of radiative transfer, enables a first order investigation of the possible influence of the molecular opacities on the time-dependent structure of the CS where the interaction with shock waves will play a role and which will be discussed in Sect. 4.2. Figs. 3 and 4 depict sequences of carbon-rich hydrostatic model structures with varying stellar temperature at constant stellar luminosity and stellar mass. The comparison of the results depicted in these figures leads to the following:

1. The inner photospheric layers are considerably less dense in the Planck models (Fig. 3) than in the Rosseland models (Fig. 4) with the same stellar parameters which certainly will influence the dust growth efficiency.
2. The varying slopes within each curve in Fig. 3 are related to the occurrence of pressure inversions in case of the Planck mean models (appearing as density inversions here) which disappear with increasing stellar temperature.
3. The different slopes in the sequence of $\rho(r)$ -curves reflect the different surface gravities.

In the sequence of Planck models shown in Fig. 3, pressure inversions are found for $T_* \leq 3000\text{K}$ ($L_* = 10^4 L_{\odot}$, $M_* = 1 M_{\odot}$, $C/O=1.8$). Only for these model parameters, a strong density enhancement of the static atmosphere due to radiation pressure on molecules is found and densities as large as

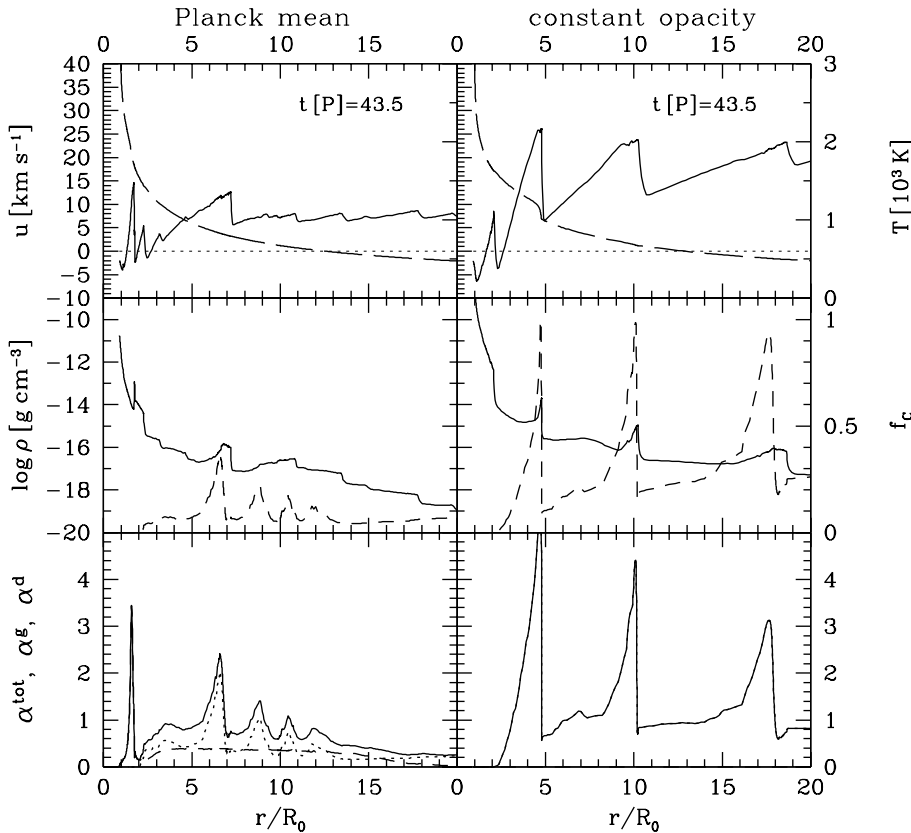


Fig. 5. Time-dependent models with different mean gas opacities. The l.h.s. depicts a Planck model and the r.h.s. a model with constant gas opacity with the **model parameters** $T_* = 3000\text{K}$, $M_* = 1M_\odot$, $L_* = 10^4 L_\odot$, $C/O = 1.8$, $\Delta u = 2\text{km s}^{-1}$, $P = 650\text{d}$ ($R_{\text{inner}} = 0.91 R_0$). **1st panels:** solid line – hydrodynamic velocity u [km s^{-1}], dashed line – gas temperature T [10^3K], dotted line – zero velocity line; **2nd panels:** solid line – gas density $\log \rho$ [g cm^{-3}], dashed line – degree of condensation f_c ; **3rd panels:** solid line – $\alpha^{\text{tot}} = a_{\text{rad}}^{\text{tot}}/g$, dashed line – $\alpha^g = a_{\text{rad}}^{\text{gas}}/g$, dotted line – $\alpha^d = a_{\text{rad}}^{\text{dust}}/g$.

10^{-15}g cm^{-3} occur at a distance of $r \approx 1.4 \dots 1.7 R_0$ (see e.g. long-dashed line, Fig. 3) already in the static case. A decrease of the luminosity or of the C/O ratio¹ hinder pressure inversion to occur. Pressure inversions are only found in the carbon-rich Planck models, but not in the oxygen-rich Planck models (not illustrated here).

4.2. Time-dependent hydrodynamic models

In Fig. 5, the hydrodynamic structure of a time-dependent carbon-rich model computed with Planck mean gas opacities is compared with a time-dependent model computed with the constant gas opacity. The radial structures can generally be separated into two distinct regions: a dust-free inner region below $\approx 2 R_0$, where dust nucleation has not yet taken place, and a dust dominated, radiatively accelerated wind region. As soon as the temperature is low enough ($T \approx 1300\text{K}$), carbon dust can form and dominates the total opacity and therefore the radiative acceleration in both models. The photospheric density structure ($r < 2 R_0$) of the Planck model exhibits a density inversion which does not exist in the model computed with a constant gas opacity (Fig. 5, 2nd panels, solid line) nor in the Rosseland models.

Dust nucleation takes place in almost the same radial zone in both models (the nucleation rate J_* is not depicted, but see

Helling 1999). Since a model computed with Planck mean gas opacities is less dense than a model with a smaller gas opacity (Fig. 5, 2nd panels, solid line), the dust growth is less efficient in the Planck model as can be seen from the smaller degree of condensation f_c (Fig. 5, 2nd panels, dashed line). The degree of condensation reaches values of $f_c \leq 40\%$ in contrast to models with a smaller gas opacity where pronounced dust layers with $f_c \geq 90\%$ are typical. Furthermore, shock waves initiated by the interior pulsation of the star are damped by the local density increase (pressure inversion; see Sect. 5.2) which leads to a less pronounced levitation of the layers beyond the pressure inverted region by shock waves.

Inspection of the total radiative acceleration α^{tot} (Fig. 5, 3rd panels, solid line) demonstrates the dominance of the dust (solid and dotted lines are identical at the r.h.s.) at $r > 2 R_0$ in both models. The molecular opacity significantly contributes to the total radiative acceleration only in the case of Planck mean gas opacities below $16 R_0$ and it dominates below $2 R_0$. At $r \approx 1.5 R_0$, the radiative acceleration by molecules reaches values as large as $3g$ which causes the local pressure inversion. The molecular opacity can contribute as much as the dust opacity if the degree of condensation $f_c \lesssim 10\%$. In contrast, the contribution of the constant gas opacity (and the Rosseland mean opacity, not shown here) to the radiative acceleration is negligible in our models.

The time-dependent Planck model depicted in Fig. 5 already exhibits a pressure inversion in the static situation which is not the case for all Planck models, e.g. those with higher stellar tem-

¹ E.g. a model with $T_* = 2800\text{K}$, $L_* = 7 \cdot 10^3 L_\odot$, $M_* = 1 M_\odot$ but $C/O=1.4$ instead of $C/O=1.8$ does not show a pressure inversion in the static case.

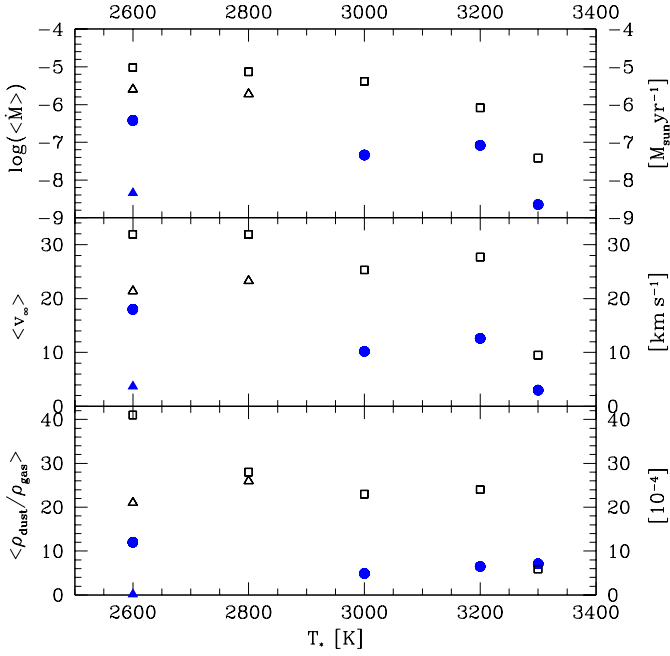


Fig. 6. Mass loss rates $\langle \dot{M} \rangle$ [$M_{\odot} \text{yr}^{-1}$], outflow velocities $\langle v_{\infty} \rangle$ [km s^{-1}], and dust-to-gas-ratios $\langle \rho_{\text{dust}} / \rho_{\text{gas}} \rangle$ [10^{-4}], are depicted for a series of models with the **model parameters** $M_{\star} = 1M_{\odot}$, $L_{\star} = 10^4 L_{\odot}$, $C/O = 1.8$, $\Delta u = 2 \text{ km s}^{-1}$, $P = 650 \text{ d}$ ($R_{\text{inner}} = 0.91 R_{\odot}$), and $T_{\star} \in [2600 \text{ K}, 3300 \text{ K}]$. Open squares - $\chi_{\text{H}}^{\text{g}} = 2 \cdot 10^{-4} \text{ cm}^2 \text{ g}^{-1}$, open triangles - $\chi_{\text{H}}^{\text{g}} = \chi_{\text{Ross}}^{\text{g}}$ (solar), filled circles - $\chi_{\text{H}}^{\text{g}} = \chi_{\text{Planck}}^{\text{g}}$ (solar), filled triangles - $\chi_{\text{H}}^{\text{g}} = \chi_{\text{Ross}}^{\text{g}}$ (LMC)

peratures: $T_{\star} = 3200 \text{ K}$ and $T_{\star} = 3300 \text{ K}$ (M_{\star} , L_{\star} , C/O , Δu , and P as in Fig. 5). In these hotter models, the temperature/density window appropriate for the high gas opacity necessary for the pressure inversion occurs only at larger radial distances which are not covered by the corresponding hydrostatic models.

4.3. Wind properties

The molecular opacities have a considerable influence on the dust complex. Since - due to the lower density - the dust growth is less efficient in the Planck models (see Sect. 4.2), the average dust-to-gas ratios $\langle \rho_{\text{dust}} / \rho_{\text{gas}} \rangle$ are smaller than those resulting from models with Rosseland mean or constant gas opacities (Fig. 6, 3rd panel). Similarly, the average outflow velocities $\langle v_{\infty} \rangle$ are smaller in the Planck models since less dust is present and acceleration by radiation pressure on dust grains is less efficient (Fig. 6, 2nd panel). The lower efficiency of dust formation in the sub-sonic region is also responsible for the small mass loss rates $\langle \dot{M} \rangle$ in the Planck models (Fig. 6, 1st panel). Similar results for these wind properties have been found by Höfner et al. (1998).

From Fig. 6 one observes furthermore, that Rosseland models (open triangles) have lower mass loss rate, outflow velocity, and dust-to-gas ratios than models computed with the constant gas opacities (open squares). This is a consequence of the Rosseland mean gas opacities being generally larger than $2 \cdot 10^{-4} \text{ cm}^2 \text{ g}^{-1}$ resulting in a globally smaller density in these models over a large range of temperatures.

For comparison, one additional model calculation with the element abundances of the LMC using Rosseland mean gas opacities is depicted in Fig. 6 (filled triangles). This model shows the smallest values of the wind properties $\langle \dot{M} \rangle$, $\langle v_{\infty} \rangle$, and $\langle \rho_{\text{dust}} / \rho_{\text{gas}} \rangle$ in the model series ($T_{\star} = 2600 \text{ K}$) since the amount of dust formed is smallest due to the smaller total amount of carbon present in the gas phase (see also Sect. 6.1).

One can set up a hierarchy from small to large molecular opacities at given metallicity with respect to the resulting wind properties: e.g. for the model series with the parameters $T_{\star} = 2600 \text{ K}$, $M_{\star} = 1M_{\odot}$, $L_{\star} = 10^4 L_{\odot}$, $C/O = 1.8$, $\Delta u = 2 \text{ km s}^{-1}$, $P = 650 \text{ d}$ ($R_{\text{inner}} = 0.91 R_{\odot}$)⁽²⁾. There is a decreasing trend of the wind properties with increasing gas opacity starting from constant gas opacity (open squares), via the Rosseland mean (open triangles), to the Planck mean gas opacities (filled circles).

Since dust growth is less effective under low-density conditions, smaller dust particles are formed. Consequently, the particles injected into the ISM would be smaller for models computed with Planck mean gas opacities than those dust particles calculated in Rosseland models or models with a constant gas opacity. The size of the particles is not unique, and multiple-peaked size distributions can occur, as discussed by Winters et al. (1999). These peaks result from different dust formation events during the history of the different gas parcels moving through the circumstellar shell.

4.4. Multi-periodicity

The phenomenon of multi-periodicity³ occurs if the eigenperiod, which is a characteristic time scale of the system induced by the formation and acceleration of dust layers, divided by the piston period yields some constant value (Fleischer et al. 1995). Models with large gas opacities (Planck models) tend to be rather semi-regular or even chaotic since less dust is formed as compared to the constant gas opacity models in Fleischer et al. (1995). In contrast to the Planck models, relatively cool ($T_{\star} < 3000 \text{ K}$) Rosseland models and constant gas opacity models have been found to be multi-periodic similar to the models presented in Fleischer et al. (1995). Since the gas opacity has an indirect but nevertheless important influence on the efficiency of dust growth, it influences the eigenperiod of the dust shell. The eigenperiod tends to increase with increasing gas opacity since the dust growth time scale is proportional to the gas density which decreases with increasing gas opacity.

5. Pressure inversions

5.1. Hydrostatic case

In hydrostatic equilibrium, $\rho g(1 - \alpha) = -\nabla P_{\text{gas}}$ holds, with P_{gas} being the gas pressure, and therefore, the occurrence of

² corresponding to Model E in Fleischer et al. (1992)

³ A model is called multi-periodic if its hydrodynamic structure periodically re-occurs after some constant time.

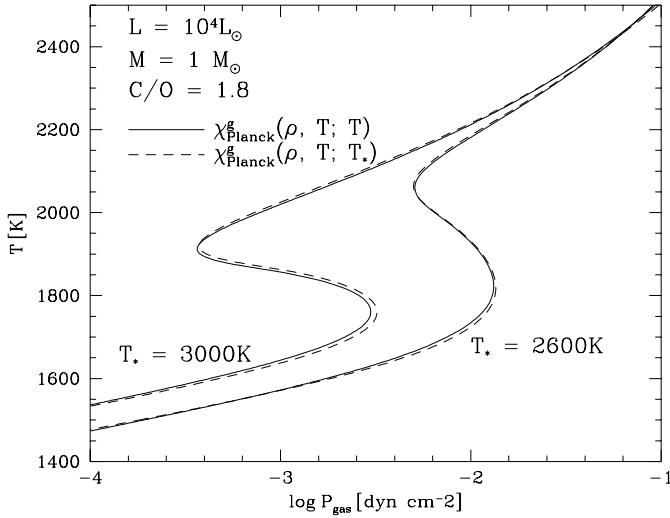


Fig. 7. The influence of the Planck mean averaging process: (T, P_{gas}) structures of Planck models computed with $\chi_{\text{H}}^{\text{g}} = \chi_{\text{Planck}}^{\text{g}}(\rho, T; T)$ (solid lines) and with $\chi_{\text{H}}^{\text{g}} = \chi_{\text{Planck}}^{\text{g}}(\rho, T; T_*)$ (dashed lines).

pressure inversions is directly related to α :

$$\begin{aligned} \alpha < 1 &\Rightarrow \frac{\partial P_{\text{gas}}}{\partial r} < 0 && \text{no gas pressure inversion} \\ \alpha > 1 &\Rightarrow \frac{\partial P_{\text{gas}}}{\partial r} > 0 && \text{gas pressure inversion,} \end{aligned}$$

One major result of the work presented here is that $\alpha > 1$ may occur due to molecular opacities alone in models with high L_* and high C/O ratios considering the Planck mean $\chi_{\text{Planck}}^{\text{g}}$ for calculating the radiative acceleration.

The occurrence of an $\alpha > 1$ in a certain parameter range of Planck models might originate from a coincidence of the maximum of the local Planck function $B(T)$ with e.g. strong molecular bands from one or several molecules (e.g. the C_2 Philips band at $1.56\mu\text{m}$ coincides with the maximum wavelength of $B(1850\text{K})$). Grey, hydrostatic models using Planck means which have been calculated from the same opacity data as described above but have been averaged according to the stellar Planck field, $\chi_{\text{Planck}}^{\text{g}} = \chi_{\text{Planck}}^{\text{g}}(\rho, T; T_*)$,

$$\chi_{\text{Planck}}^{\text{g}}(\rho, T; T_*) = \frac{\int \chi_{\nu}^{\text{g}}(\rho, T) B_{\nu}(T_*) d\nu}{\int B_{\nu}(T_*) d\nu}, \quad (1)$$

have been compared with hydrostatic models computed with Planck means calculated according to the local Planck field, $\chi_{\text{Planck}}^{\text{g}} = \chi_{\text{Planck}}^{\text{g}}(\rho, T; T)$ (Fig. 7).

Since the local, monochromatic opacities are weighted by either the local or the stellar Planck field in the two averaging procedures, respectively, and both produce a very similar model structure, a specific coincidence of strong absorption coefficients with the maximum of the Planck function can be excluded as the predominant cause for the occurrence of pressure inversions.

Fig. 8 depicts two sets of initial models with different stellar temperature, $T_* = 2600\text{K}$ and $T_* = 3000\text{K}$ (L_* , M_* , C/O see figure) for which the importance of single opacity species has

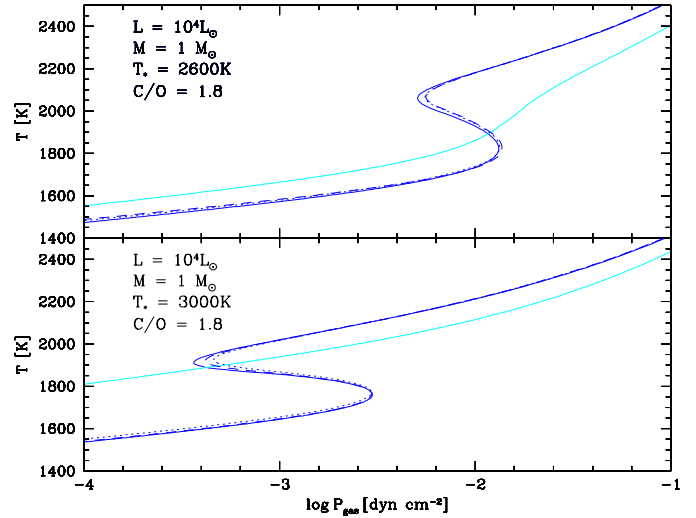


Fig. 8. The importance of single line opacity species for the formation of pressure inversions. The static models have been calculated i) including all molecules as opacity species (full black line), ii) excluding C_3 (dotted line), iii) excluding C_2H_2 (dashed line), and iv) excluding C_2 (full grey line).

been investigated. The solid lines indicate the model computations including all opacity species (reference model). In the other models depicted, single molecular opacity species have been left out in order to test whether a molecule can be identified as the main contributor to the local gas opacity responsible for the pressure inversion. The major effect on the (T, P_{gas}) structure of the static models result from the neglect of C_2 as opacity contributor (grey line) in both model sets. The neglect of C_2 causes the pressure inversion to vanish. The second most important molecule regarding the pressure inversion is C_3 (dotted line). For $T_* = 2600\text{K}$, C_3 (dotted line) and C_2H_2 (dashed line) influence the model structure with similar strength. The neglect of the HCN opacity results in a change of the model structure comparable to C_2H_2 and is therefore not depicted here.

These results are confirmed by an analysis of the monochromatic gas opacity at a typical $(T, n_{\text{(H)}})$ point in the pressure inversion domain depicted in Fig. 9. The plot labelled with ‘all molecules +cont.’ shows the monochromatic gas opacity at $T = 2000\text{K}$ and $n_{\text{(H)}} = 10^{10}\text{cm}^{-3}$ including all line and continuum opacities, as well as scattering which dominates at long wavelengths. The other plots depict the monochromatic line opacity of single species plus the continuum opacity. One easily notices that CH, C_2H_2 , and HCN have very small opacities due to very small concentrations and do therefore not contribute significantly to the Planck mean opacity of the gas at that $(T, n_{\text{(H)}})$ point. CO contributes with its three strong vibrational bands. Its contribution is, however, limited to narrow wavelength intervals. In contrast, the opacity of C_2 is remarkably large at almost all wavelengths and contributes therefore strongly to the total Planck mean and thereby to the occurrence of the pressure inversion. The contributions of CN and C_3 are comparable in strength but occur in different wavelength regions. C_3 provides, however, the main contribution to the total

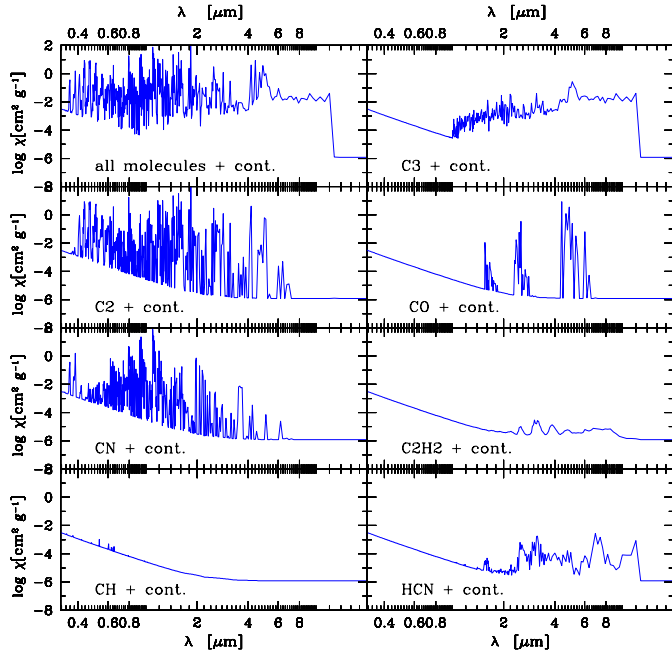


Fig. 9. Monochromatic gas opacities at $T = 2000\text{K}$, $n_{(\text{H})} = 10^{10}\text{cm}^{-3}$. Also the single molecule’s opacities are shown together with the continuum contributions.

opacity at long wavelengths whereas CN is most important at the short wavelength end.

Investigations have shown that, although C_3 has a number density at least one order of magnitude larger than the other opacity species in the $(T, n_{(\text{H})})$ domain of the pressure inversions, C_3 does not necessarily yield the main contribution to the Planck mean opacity.

5.2. Hydrodynamic case

The piston creates waves which rapidly steepen into strong shocks in the exponential density gradient of the photosphere. These shock waves enter into the pressure inverted zone. In Fig. 10, the interaction between shock waves and a pressure inverted region is shown. The l.h.s. column depicts the static, unperturbed case $u = 0$ (labelled with “static”). One observes that the opacity peak in the lower panel coincides with the increasing density in the static situation. The density inversion is similar to the one shown in Fig. 3.

The next three columns of Fig. 10 depict the perturbed case of the hydrodynamic model for three subsequent instants of time. The second column ($t = 43.5 P$) shows a strong shock wave at $R \approx 1.7 R_0$ running into the density inversion and causing a strong compression of this gas. At the same time momentum is transferred to the gas and the gas is accelerated outward. As the gas moves outward, the temperature decreases and since the opacity was at maximum before, it will decrease due to the changing thermodynamic conditions. Consequently, the opacity peak does not coincide any more with the ascending branch of the density inversion at $t = 43.5 P$.

In the third column ($t = 43.7 P$) the shock wave has partly transferred its energy to the gas causing an extension of this region of enhanced density towards larger radial distances. The shock wave has split into two parts: one remaining in front of the density inversion ($R \approx 1.7 R_0$, *reflected part*) and one travelling further outwards with decreased amplitude ($R \approx 1.95 R_0$, *transmitted part*).

At the fourth instant of time ($t = 43.9 P$), the initial shock wave has been totally split into two waves with different velocity amplitudes ($R \approx 2.2 R_0$, $R \approx 1.5 R_0$) which are strongly reduced in comparison to the initial shock wave. The reflected, inward travelling shock wave ($R \approx 1.6 R_0$) leads to negative velocities. The infall of the gas is stopped as soon as the material reaches thermodynamic conditions where the gas opacity increases again and the radiation pressure counterbalances the gravitational deceleration. This situation is depicted in the fourth column of Fig. 10, where the negative velocity, the branch of increasing density, and the opacity peak coincide in space and time. The initial, unperturbed situation re-occurs, i.e. a layer of high density again “swims” on the radiation field due to its large opacity.

Pressure inversions can also occur independent of the gas opacity in layers where dust is formed (consult e.g. the models in Fleischer et al. 1992; Winters et al. 1997; Höfner & Dorfi 1997). In such models, the local increase of the density with increasing distance from the star is a result of the strong dust opacity, which by radiation pressure causes a compression of the material just behind the shock front (Fig. 5).

6. Discussion

6.1. Wind properties

Piston amplitude: Molecular opacities indirectly influence the mass loss rate, outflow velocity and dust-to-gas ratio since an increasing gas opacity causes an atmosphere to be less dense resulting also in a less efficient dust growth and thereby in reduced wind properties. The globally decreased gas density due to a higher gas opacity can partly be compensated by an increasing piston amplitude Δu as discussed by Fleischer et al. (1992) and Höfner et al. (1998). From the work presented here, we find that the wind properties resulting from models computed with a constant gas opacity have to be considered as an upper limit. The mass loss formula of Arndt et al. (1997) therefore serves as an upper limit estimation of the mass loss rate for given stellar parameters in the particular range where this formula applies.

Carbon-to-Oxygen ratio: Considering increasing C/O ratios in a carbon-rich gas, a sensitive competition of two effects with opposite influence on the dust complex exists. With increasing C/O ratio, the gas opacity further increases causing the overall gas density to decrease which worsens the conditions for effective dust formation in such models (see also Höfner et al. 1998). On the other hand, the concentrations of the carbon-bearing molecules increase with increasing C/O ratio which improves the conditions for dust formation and results in larger outflow ve-

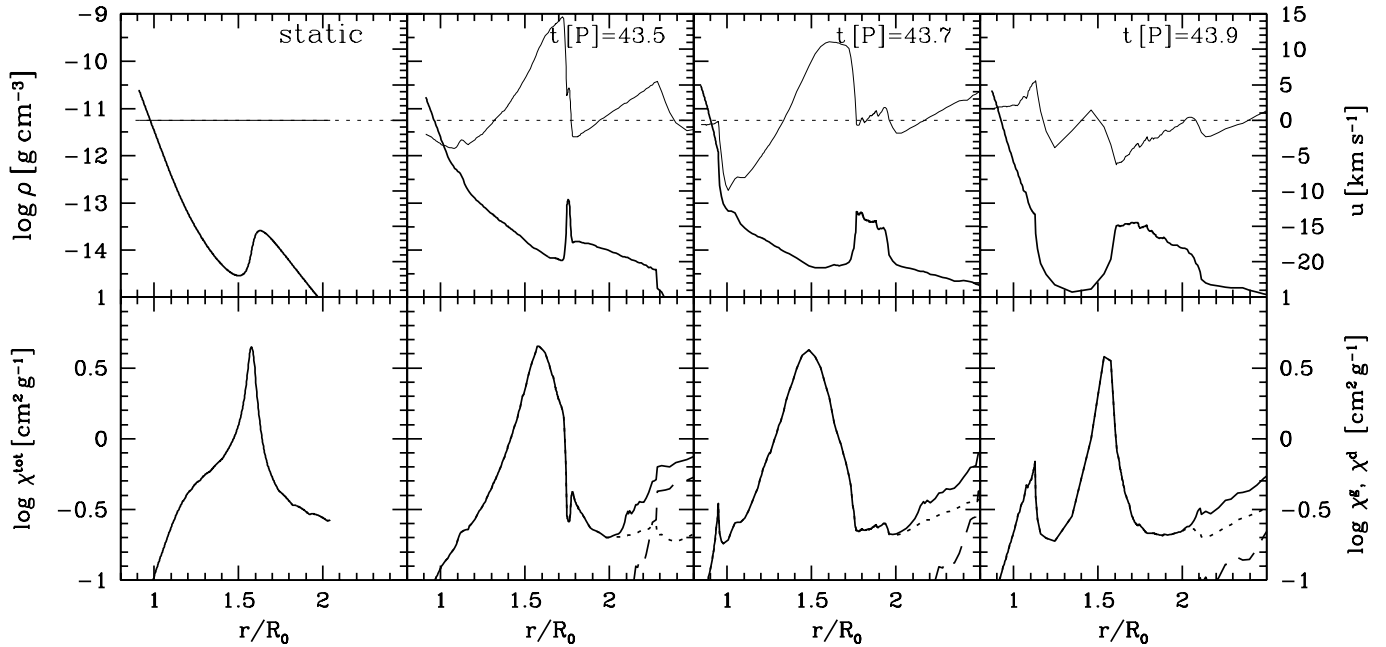


Fig. 10. The interaction of pressure inversions and shock waves. The **model parameters** are $T_* = 3000\text{K}$, $M_* = 1M_\odot$, $L_* = 10^4L_\odot$, $C/O = 1.8$, $\Delta u = 2\text{km s}^{-1}$, $P = 650\text{d}$, $R_{\text{inner}} = 0.91 R_0$ (see Fig. 5). **1st row:** thick solid line – gas density ρ [g cm^{-3}], thin solid line – hydrodynamic velocity u [km s^{-1}], dotted line – zero velocity line; **2nd row:** solid line – total opacity χ^{tot} [cm^2g^{-1}], dotted line – gas opacity χ^g [cm^2g^{-1}], dashed line – dust opacity χ^d [cm^2g^{-1}].

locities (Fleischer 1994; Arndt et al. 1997). Also from Table 1 in Höfner et al. (1998) one observes that a pure increase of the C/O ratio with otherwise constant model parameters leads to a considerably larger terminal wind velocity.

Metallicity: A decrease of the fraction of metals in the gas causes a decrease of the wind properties since it directly influences the amount of dust formed. This effect can be compensated if such stars have either larger C/O ratios, larger pulsation amplitudes and/or larger stellar luminosities compared to stars in the solar neighbourhood.

Observations indeed give evidence that a significant number of large amplitude variables exist in the Magellanic Clouds with considerably higher luminosities than those of the solar neighbourhood (van Loon et al. 1999; Whitelock & Feast 1999).

Dust opacity: In the present paper we discuss the influence of molecular opacities on the wind properties of pulsating cool, carbon-rich stars. Recently, Andersen et al. (1999) have investigated the influence of different mean carbon dust opacities on the wind properties of time-dependent hydrodynamic models. In contrast to the gas opacity, no significant influence of the dust opacity on the mass loss rate $\langle \dot{M} \rangle$ has been found. The outflow velocity $\langle v_\infty \rangle$ decreases with decreasing dust extinction and the mean degree of condensation⁴ increases. Fleischer et al. (1999) have presented a similar study regarding the influence of dust extinction data on the properties of time-dependent

⁴ $\langle f_c \rangle = \langle \rho_{\text{dust}} / \rho_{\text{gas}} \rangle \sum_i m_i n_i^g / m_C n_C^d$ (n_C^d is the number density of condensable material)

models which have been computed with a constant gas opacity. The results are similar to Andersen et al. (1999): $\langle \rho_{\text{dust}} / \rho_{\text{gas}} \rangle$ generally increases while $\langle v_\infty \rangle$ decreases with decreasing dust extinction since the dust grains have more time to grow.⁵ The mass loss rate does not follow such a clear trend. However, the results regarding the wind properties obtained with the 7 different data sets investigated by Fleischer et al. (1999) show a larger scattering than the results obtained by Andersen et al. (1999). Note that the data sets in Fleischer et al. (1999) and Andersen et al. (1999) are different.

The dependence of the wind properties on the dust extinction stays in contrast to their dependence on the gas opacity: $\langle \dot{M} \rangle$, $\langle v_\infty \rangle$, $\langle \rho_{\text{dust}} / \rho_{\text{gas}} \rangle$ decrease with increasing gas extinction.

6.2. Pressure inversions

Existence of pressure inversions: Asplund (1998) has observed pressure inversions in the inner parts of non-grey hydrogen-deficient hydrostatic MARCS model computations and pressure inversions have also been found in the inner regions of non-grey metal-poor hydrostatic MARCS model atmospheres (Helling 1996, e.g. Fig. 7.2). In all these models, the positive pressure gradient stabilises the atmosphere which locally exceeds $\alpha = 1$. Asplund (1998) explains the occurrence of the gas pressure

⁵ The dust extinction data for amorphous carbon used in Fleischer et al. (1999) arrange from large to small Planck mean values like AC1, BE1, HAPS1, FC21PS (Rouleau & Martin 1991), MARONAC (Maron 1990), POYHAC (Preibisch et al. 1993), and the smallest is MWAC (Mathis & Whiffen 1989).

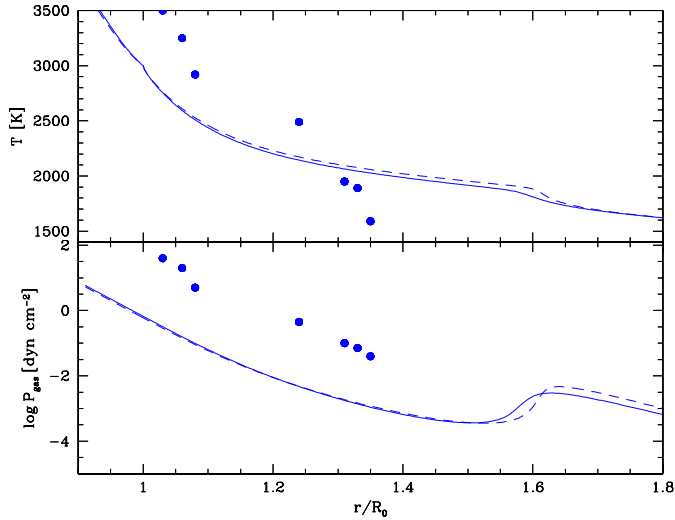


Fig. 11. Comparing a hydrostatic Planck model (solid line, $C/O = 1.8$) with a frequency-dependent, hydrostatic model by Scholz & Tsuji (1984) (black dots, $C/O = 2.0$) and a Planck model without C_3 (dashed line, $C/O = 2.0$). **Model parameter:** $T_{\star} = 3000\text{K}$, $M_{\star} = 1M_{\odot}$, $L_{\star} = 10^4L_{\odot}$.

inversion in their models by the high continuum opacity in the He ionisation zone.

Achmad et al. (1997), who investigated stationary wind models of supergiants, arrived at the same conclusion, namely, that pressure inversions are real and not an artifact of the hydrostatic assumption since the inversion remains in the stationary model computation. Achmad et al. (1997) have used the hydrostatic $T(\tau)$ structures from Kurucz which already exhibit pressure inversions (see Table 1 in Achmad et al. 1997).

Jørgensen & Johnson (1992) argued that frequency-dependent cool star hydrostatic model atmospheres cannot produce $\alpha > 1$ due to the quality of the present absorption coefficient data and the neglect of practically unknown absorption coefficients. The basis for this conclusion, however, was the assumption that the line center frequencies are constant at every depth in the atmosphere. Jørgensen & Johnson (1992) concluded that in a dynamic atmosphere, the value of the radiative acceleration a_{rad} would be larger because large χ_{ν} would be continuously shifted to neighbouring frequencies where higher fluxes H_{ν} can be received. Hence, a_{rad} can be larger in a dynamic atmosphere than in a static atmosphere, because large absorption coefficients may combine with high flux values. Jørgensen & Johnson (1992) calculated models with artificially increased molecular absorption (factors of 5 to 7) where they found that the maximum α increases from 0.15 to values larger than 1 for models with $T_{\text{eff}} = 2500\text{K} \dots 2800\text{K}$, $\log g = -1.0$, and $C/O=2.0$. For a model $T_{\text{eff}} = 3100\text{K}$, $\log g = -0.5$, and $C/O=2.0$ a factor of 10 was needed to increase α to values larger than one.

Comparison with static, frequency-dependent models: In order to put the Planck models in a comparative frame, a typical non-grey, hydrostatic model computed by Scholz & Tsuji (1984) has been compared to a static Planck model.

Fig. 11 depicts an initial, grey, hydrostatic Planck model (solid line, $C/O=1.8$) and an extended, carbon-rich, non-grey hydrostatic model (Scholz & Tsuji 1984) (black dots, $C/O=2.0$). Both models are spherical symmetric and have the same stellar parameter but a different C/O ratio. In addition, a Planck model is depicted where C_3 has been left out in the opacity computation (dashed line, $C/O=2.0$) since also the model calculated by Scholz & Tsuji (1984) does not contain the C_3 opacity. The temperature and the gas pressure as function of the radial distance are very similar for the Planck models with $C/O=1.8$ (solid line) and with $C/O=2.0$ (dashed line, without C_3). We can therefore compare the Planck model with $C/O=1.8$, which has widely been used in this paper, with the non-grey, hydrostatic model of Scholz & Tsuji (1984).

The basic (T, P_{gas}, r) structure of the static, frequency dependent model is reasonably represented by the Planck model(s). Höfner et al. (1998) have shown a similar comparison between an initial Planck model and a frequency-dependent, hydrostatic model obtained with the MARCS code (e.g. Jørgensen et al. 1992). The models compared by Höfner et al. (1998) ($T_{\star} = 2880\text{K}$, $L_{\star} = 7 \cdot 10^3 L_{\odot}$, $M_{\star} = 1 M_{\odot}$, $C/O=1.4$) exhibit similar differences in the (T, P_{gas}) plane as the models depicted in Fig. 11.

Fig. 11 demonstrates also that the Planck models are much more extended than the frequency-dependent model due to the generally larger mean opacity at every location in the atmosphere (see also Jørgensen 1994). Thereby, the pressure inversion is located at radial positions which are not covered by the non-grey model.

The results of such a comparison must be taken with care since the velocity fields very likely tend to abolish the anti-correlation between the frequency dependent opacity χ_{ν} and the flux H_{ν} present in static models. Consequently, the Planck mean (uncorrelated weighting) is apparently a better choice than the Rosseland mean (anti-correlation weighting) for time-dependent models.

It should, however, be noted that the time-dependent modelling including dust formation can presently not be performed with a frequency resolution comparable to the hydrostatic models (e.g. Gustafsson et al. 1975; Scholz & Tsuji 1984; Jørgensen 1989; Plez et al. 1992; Allard & Hauschildt 1995) because of the immense numerical effort.

Under these circumstances, the reality of density inversions may still be considered as an unsolved problem which definitely deserves future investigations in terms of a frequency-dependent, hydrodynamic model calculation which includes the effect of Doppler shifts of the molecular lines.

Interaction with shock waves: The interaction between shock waves and pressure inversions has been lined out in Mihalas & Weibel Mihalas (1984): travelling waves are partly reflected and partly transmitted, i.e. they “tunnel” through the dense layer and continue to propagate outwards with a reduced amplitude beyond the pressure inverted region. Shocks may also split into two waves of almost similar strength: one continues to travel

outwards, one travels backwards which will merge with the subsequent shock. Partial wave reflection can also be observed from the model series described in Fleischer et al. (1992, 1995) and Winters et al. (1994).

Rayleigh-Taylor instabilities: The interface of a gas where the radiative acceleration balances or even exceeds the gravitational acceleration might be thought to be Rayleigh-Taylor unstable⁶ since here a layer of high density “swims” on the radiation field due to its large opacity. Hence, pressure inversion might a priori thought to be Rayleigh-Taylor unstable. Since at the ascending branch of the pressure inversions also the direction of the total local acceleration is reversed, the criteria for a Rayleigh-Taylor instability are not fulfilled in the static case (see the stability analysis by Wentzel 1970). In the dynamic case where the radiation pressure or the acceleration by a shock wave might locally be not large enough to overcome the gravitational deceleration, the ascending branch will be Rayleigh-Taylor unstable and the net motion of the gas is towards the star (Fig. 10, $t = 43.7, 43.9$) until it is stopped again by a counteracting force. This transition from an unstable to a stable situation is described in one dimension by the time-dependent model as depicted in Fig. 10. In order to resolve possible effects like clumpy or finger-like structures related to Rayleigh-Taylor unstable gases, multi-dimensional modelling of such a hydrodynamic situation is necessary which go beyond the scope of this paper. Results of such studies concerning the collision of a fast and a slow wind from red giants in the outer circumstellar shell have been presented by e.g. Gustafsson et al. (1999).

7. Conclusions

New Planck and Rosseland mean gas opacity tables have been calculated for temperatures $T \in [500\text{K}, 10\,000\text{K}]$, total hydrogen densities $n_{(\text{H})} \in [10^5\text{cm}^{-3}, 10^{15}\text{cm}^{-3}]$ and various element abundances including the molecular line opacities for CO, TiO, SiO, H₂O, CH, CN, C₂, C₃, HCN, and C₂H₂ beside several continuum sources. Both mean opacities are similar at high temperature where continuum absorption dominates. However, differences of up to 3 orders of magnitude occur at low temperatures in the molecular domain caused by the strong frequency dependence of the molecular opacities. The analysis of the mean opacities has shown that the oxygen-bearing molecular opacity species TiO, SiO, and H₂O can contribute below 1000 K to the Planck mean gas opacities but not to the Rosseland mean gas opacities of a carbon-rich gas.

Molecular opacities play an important role for the structure and the dynamics of the winds of AGB stars. First, the molecular opacities determine the overall density-level of the stellar

⁶ Rayleigh-Taylor instabilities occur if a medium 1 with a density ρ_1 is supported by a medium 2 with a density ρ_2 in a gravitational field ($\rho_1 > \rho_2$), or equivalently, when a heavy medium is accelerated by a light medium. Rayleigh-Taylor instabilities are known from a wide range of astrophysical phenomena and/or objects, e.g. accretion onto compact objects, supernova explosions or shock waves interacting with interstellar clouds (see for instance Jun et al. 1996).

atmosphere, which forms the foot point for any stellar outflow. Consequently, the molecular opacity has an important, indirect influence also on the amount of dust formed in the CS. Second, molecules can exert a significant force on the gas due to radiation pressure.

The hydrodynamic structure found in the time-dependent models can roughly be separated into two distinct regions: a region dominated by molecules at small radial positions (*molecular domain*) and a region dominated by dust at larger radii, $r > 2 \dots 3 R_0$, (*dust domain*). Large gas opacities in the *molecular domain* can result in a radiative acceleration which exceeds the gravitational deceleration ($\alpha^{\text{tot}} > 1$) in Planck models. As a consequence, a pressure inverted zone can be present for certain stellar parameters and its occurrence in the time-dependent models at $r \lesssim 2 R_0$ proves that the positive pressure gradient in the initial models is not an artifact of the hydrostatic equilibrium, but is rather a consequence of the physical situation encountered by the system.

A positive pressure gradient in hydrostatic model atmospheres indicates that $\alpha > 1$ does not necessarily lead to an outflow of atmospheric material as long as the system is able to compensate for the increasing radiative acceleration. Therefore, the occurrence of LOCAL gas pressure inversions does not violate the global assumption of hydrostatic equilibrium, since the locally increased gas pressure is stabilised by surrounding material with smaller opacity, and the gas pressure vanishes at infinity as it is demanded for physical reasons.

We conclude that the radiation pressure on molecules does NOT directly contribute to the wind driving mechanism in the models discussed here but molecular opacities do influence the efficiency of the driving mechanism by worsening the conditions for dust growth: the Planck models (i.e. models with large opacities) generally exhibit lower mass loss rates, lower outflow velocities, and lower dust-to-gas ratios than models using Rosseland mean or constant gas opacities. The wind properties resulting from Planck models can therefore be considered as the lower limit for the actual wind properties for given metallicity. A decrease of the metallicity (e.g. for LMC abundances) generally causes a reduction of the mass loss rate, the outflow velocity and the dust-to-gas ratio. A larger C/O ratio and/or higher luminosities are required in order to provide mass loss rates comparable to the solar neighbourhood.

Time-dependent models of circumstellar dust shells with a strong molecular absorption component seem to exhibit rather a chaotic than a multi-periodic behaviour, but more detailed investigations are needed to clarify this point.

Acknowledgements. We thank the referee Dr. T. Tsuji for his valuable comments and suggestions on the manuscript. Useful comments from Dr. P. Woitke are gratefully acknowledged. This work has been supported by the *FAZIT-Stiftung*, the *BMBF* (grant 05 3BT13A 6) and partly by the *DFG* (grant Se 420/15-1). The calculations were performed on the Cray computers of the Konrad-Zuse-Zentrum für Informationstechnik Berlin (ZIB).

Appendix A: Element abundances

elem.	solar		LMC	SMC	
	$\epsilon_{\text{el}}^{\text{solar}}$	ref.	$\epsilon_{\text{el}}^{\text{LMC}}$	$\epsilon_{\text{el}}^{\text{SMC}}$	ref.
H	12.00	AG89	12.00	12.00	RD92
He	10.99	"	10.94	10.91	"
C	8.60	G91	8.04	7.73	"
N	7.97	GN93	7.14	6.63	"
O	8.87	"	8.35	8.03	"
Ne	8.07	"	7.61	7.27	"
Na	6.33	AG89	7.15	5.96	"
Mg	7.58	"	7.47	6.98	"
Al	6.47	"	[solar] ^[a]	6.40	AG89 RD92
Si	7.55	"	7.81	7.03	RD92
S	7.21	"	6.70	6.59	"
K	5.12	"	[solar] ^[a]	[solar] ^[a]	AG89
Ca	6.36	"	5.89	5.69	RD92
Cr	5.67	"	5.47	5.10	"
Mn	5.39	"	5.21	5.03	"
Fe	7.51	"	7.23	6.84	"
Ni	6.25	"	6.04	5.85	"
Ti	4.93	B92	4.81	4.49	"

Table A.1. Logarithmic element abundances used in this work. The abbreviations refer to: AG89 – Anders & Grevesse (1989), G91 – Grevesse et al. (1991), GN93 – Grevesse & Noels (1993), B92 – Bizzarri et al. (1992), RD92 – Russel & Dopita (1992).

^[a] LMC and SMC values for Al and K were not available, therefore, the solar element abundances have been used.

Appendix B: TiC equilibrium constant

The logarithmic pressure equilibrium constant $\log K_p = \log(p(A)^a p(B)^b / p(A_a B_b))$ with A and B being the atomic constituents of the molecule $A_a B_b$, and a and b the stoichiometric factors, is given as a fourth-order polynomial in $\theta = 5040/T$:

$$\log K_p(T) = c_0 + c_1 \theta + c_2 \log(\theta) + c_3 (\log \theta)^2 + c_4 (\log \theta)^3. \quad (\text{B.1})$$

The equilibrium constant K_p has been estimated from spectroscopic data (McFeaters et al. 1994) by A. Gauger (priv. comm.) and the coefficients are

$$c_0 = 12.75293 \quad c_1 = -5.4485 \quad c_2 = -1.56672 \\ c_3 = 1.56041 \quad c_4 = -0.93275$$

References

- Achmad L., Lamers H., Pasquini L., 1997, A&A 320, 196
 Alexander D.R., Johnson H.R., Rypma R.L., 1983, ApJ 272, 773
 Allard F., Hauschildt P.H., 1995, ApJ 445, 433
 Anders E., Grevesse N., 1989, Geochimica et Cosmochimica Acta 53, 197
 Andersen A., Loidl R., Höfner S., 1999, A&A 349, 243
 Arndt T.U., Fleischer A.J., Sedlmayr E., 1997, A&A 327, 614
 Asplund M., 1998, A&A 330, 641
 Bizzarri A., Huber M., Noels A., et al., 1993, A&A 273, 707
 Bowen G.H., 1988, ApJ 329, 299
 Carbon D., Gingerich O., Latham D., 1969, In: Kumar S. (ed.) Low Luminosity Stars. Gordon and Breach, New York
 Castor J.L., Abbott C., Klein R.I., 1975, ApJ 195, 157
 Chase Jr. M.W., Davies C.A., Downey Jr. J.R., et al., 1985, In: J. Phys. Chem. Ref. Dat. Vol. 14, Suppl. 1, National Bureau of Standards
 Dalgarno A., 1962, The Scattering of light by Atomic Systems. Volume III of Spectral Reflectivity of the Earth Atmosphere. Geoph. Corp. of America
 Doyle R., 1968, The continuous spectrum of the hydrogen quasi-molecule. Ph.D. Thesis, Harvard University, Harvard, USA
 Feuchtinger M.U., Dorfi E.A., Höfner S., 1993, A&A 273, 513
 Fleischer A.J., Gauger A., Sedlmayr E., 1992, A&A 266, 321
 Fleischer A.J., 1994, Hydrodynamics and Dust Formation in the Circumstellar Shells of Miras and Long-Period Variables. Ph.D. Thesis, Technische Universität, Berlin, FRG
 Fleischer A.J., Gauger A., Sedlmayr E., 1995, A&A 297, 543
 Fleischer A.J., Winters J.M., Sedlmayr E., 1999, In: Le Bertre T., Lèbre A., Waelkens C. (eds.) IAU Symp. 191, AGB stars. ASP Conf. Ser., p. 187
 Gail H.-P., Sedlmayr E., 1985, A&A 148, 183
 Gail H.-P., Sedlmayr E., 1986, A&A 166, 225
 Gail H.-P., Sedlmayr E., 1988, A&A 206, 153
 Gail H.-P., Keller R., Sedlmayr E., 1984, A&A 133, 320
 Gauger A., Gail H.-P., Sedlmayr E., 1990, A&A 235, 345
 Goorvitch D., Chackerian Jr. C., 1994, ApJS 91, 483
 Grevesse N., Noels A., 1993, In: Origin and evolution of the elements. University Press, Cambridge, p. 14
 Grevesse N., Lambert D., Sauval A., van Dishoeck E., Farmer C., 1991, A&A 242, 488
 Gustafsson B., Bell R.A., Eriksson K., Nordlund Å., 1975, A&A 42, 407
 Gustafsson B., Myasnikov A., Eriksson K., 1999, In: Hron J., Höfner S. (eds.) Atmospheres of M, S and C Giants. 2nd Austrian ISO Workshop, p. 99
 Hashimoto O., 1995, ApJ 442, 286
 Helling Ch., 1996, Master's thesis, TU Berlin and Niels Bohr Institut Copenhagen (<http://export.physik.TU-Berlin.DE/~chris/>)
 Helling Ch., 1999, Role of molecular opacities in circumstellar dust shells. Ph.D. Thesis, TU Berlin, FRG
 Helling Ch., Jørgensen U.G., 1998, A&A 337, 477
 Höfner S., 1999, A&A 346, L9
 Höfner S., Dorfi E.A., 1997, A&A 319, 648
 Höfner S., Jørgensen U.G., Loidl R., Aringer B., 1998, A&A 340, 497
 John T., 1988, A&A 193, 189
 Jørgensen U.G., 1989, ApJ 344, 901
 Jørgensen U.G., 1990, A&A 232, 420
 Jørgensen U.G., 1994, In: Jørgensen U.G. (ed.) Molecules in the Stellar Environment. Springer, Berlin, p. 29
 Jørgensen U.G., Jensen P., 1993, J. Mol. Spect. 161, 219
 Jørgensen U.G., Johnson H.R., 1992, A&A 265, 168
 Jørgensen U.G., Larsson M., 1990, A&A 238, 424
 Jørgensen U.G., Almlöf J., Siegbahn P.E.M., 1989, ApJ 343, 554
 Jørgensen U.G., Johnson H.R., Nordlund Å., 1992, A&A 261, 263
 Jørgensen U.G., Larsson M., Iwamae A., Yu B., 1996, A&A 315, 204
 Jun B.-I., Jones T., Norman M., 1996, ApJ 468, L59
 Karzas W., Latter R., 1961, ApJS 6, 167
 Kurucz R., 1979, ApJS 40, 1
 Langhoff S., Bauschlicher Jr. C., 1993, Chem. Phys. Letters 211(4,5), 305

- van Loon J.T., Groenewegen M.A.T., de Koter A., et al., 1999, *A&A* 351, 559
- Maciel W.J., 1976, *A&A* 48, 27
- Maron N., 1990, *Ap&SS* 172, 21
- Mathis J.S., Whiffen G., 1989, *ApJ* 341, 808
- McFeaters J., Stephens R., Schwerdtfeger P., Liddell M., 1994, *Plasma Chemistry and Plasma Processing* 14, 333
- Mihalas D., 1965, *ApJS* 9, 321
- Mihalas D., Weibel Mihalas B., 1984, *Foundations of Radiation Hydrodynamics*. Oxford University Press
- Pauldrach A.W.A., Puls J., Kudritzki R.P., 1986, *A&A* 164, 86
- Peach G., 1970, *Mem. R. Astron. Soc.* 73, 1
- Plez B., Brett J.M., Nordlund A., 1992, *A&A* 256, 551
- Preibisch T., Ossenkopf V., Yorke H.W., Henning T., 1993, *A&A* 279, 577
- Rouleau F., Martin P.G., 1991, *ApJ* 377, 526
- Russel S., Dopita M., 1992, *ApJ* 384, 508
- Scholz M., Tsuji T., 1984, *A&A* 130, 11
- Snedden C., Johnson H., 1976, *ApJ* 204, 281
- Somerville W.B., 1964, *ApJ* 139, 192
- Tsuji T., 1973, *A&A* 23, 411
- Unno W., Kondo M., 1976, *PASJ* 28, 347
- Unno W., Kondo M., 1977, *PASJ* 29, 693
- Wentzel D., 1970, *ApJ* 160, 373
- Whitelock P., Feast M., 1999, *Mem. Soc. Astron. Ital.*, in press
- Winters J.M., Fleischer A.J., Gauger A., Sedlmayr E., 1994, *A&A* 290, 623
- Winters J.M., Fleischer A.J., Le Bertre T., Sedlmayr E., 1997, *A&A* 326, 305
- Winters J.M., Le Bertre T., Keady J.J., 1999, In: Le Bertre T., Lèbre A., Waelkens C. (eds.) *Asymptotic Giant Branch Stars*. IAU Symp. 191, ASP, p. 261